High Efficiency Plastic Scintillator Detector with Wave-Length Shifting Fiber Readout for the GLAST Large Area Telescope

A. A. Moiseev[1], P. L. Deering[2,], R. C. Hartman[3], T. E. Johnson[3], T. R. Nebel[2], J. F. Ormes[4], and D. J. Thompson[3]*

[1] CRESST and Astroparticle Physics Laboratory NASA/GSFC, Greenbelt, MD 20771
[2] Fermi National Accelerator Laboratory, Batavia, IL 60510
[3] NASA/Goddard Space Flight Center, Greenbelt, MD 20771
[4] University of Denver, Denver, CO 80208
[*] retired

Abstract.
This paper describes the design and performance studies of the scintillator tile detectors for the Anti-Coincidence Detector (ACD) of the Large Area Telescope (LAT) on the Gamma ray Large Area Space Telescope (GLAST), scheduled for launch in early 2008. The scintillator tile detectors utilize wavelength shifting fibers and have dual photomultiplier tube (PMT) readout. The design requires highly efficient and uniform detection of singly charged relativistic particles over the tile area and must meet all requirements for a launch, as well as operation in a space environment. We present here the design of three basic types of tiles used in the ACD, ranging in size from ~450 cm^2 to ~2500 cm^2, all 1 cm thick, with different shapes, and with photoelectron yield of ~20 photoelectrons per minimum ionizing particle (mip) at normal tile incidence, uniform over the tile area. Some tiles require flexible clear fiber cables up to 1.5 m long to deliver scintillator light to remotely located PMT.

1. Introduction

The scintillating tile detectors are key elements of the Large Area Telescope (LAT) Anti-Coincidence Detector (ACD). The LAT [1] is scheduled for launch early in 2008 as the main instrument of a new gamma-ray observatory GLAST. LAT will detect celestial gamma-rays in the energy range from ~ 20 MeV to > 300 GeV with angular, energy, and time resolution substantially better than in its predecessor EGRET on the Compton Gamma Ray Observatory [2]. A detailed description of the ACD is given in [3] where most aspects of the system design, fabrication and tests are covered. The purpose of this paper is to provide the design details for the ACD main component, the scintillator tile detector, and its readout.

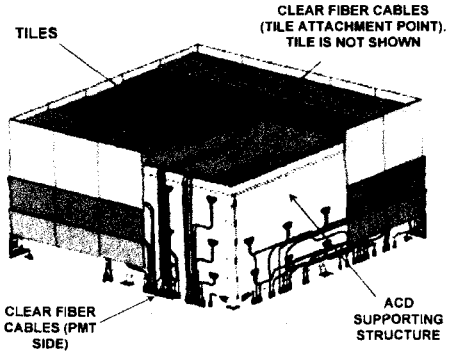

Figure 1. ACD structure. The long tiles are not shown. PMTs (not shown) are located around the bottom edge of the ACD

The main purpose of the ACD is to detect charged particles efficiently and to create a veto signal that can be used to reject charged particles. The ACD is a square 1.7m x 1.7m x 0.9m hat covering the top and four sides of the LAT (Fig. 1). The flux of charged particles in the GLAST orbit exceeds the flux of gamma-rays by 3-5 orders of magnitude, and the ACD has the primary responsibility for eliminating that charged particle background. This requires that the ACD efficiency for detecting singly charged relativistic particles (minimum ionizing particles, or MIP) be > 0.9997, averaged over its entire area of 8.3 m^2. The LAT is required to be sensitive to photons up to 300 GeV in spite of the presence of backsplash from the electromagnetic showers created by the high energy gamma rays in the LAT calorimeter (Compton electrons made by ~0.5 MeV photons in the shower). The higher the primary photon energy, the more intense the backsplash is, so the approach is to "divide and conquer". The ACD is segmented into an array of 89 separate tiles reducing the probability that the track (in the Tracker subsystem) points back to a scintillating tile with a signal from a backsplash photon (see [3] and [4] for more details). The background particles are isotropic except for shadowing effects of the Earth and its magnetic field. In order to detect particles over all parts of the LAT field of view, we must minimize the "dead" areas, those without active detectors. These dead areas include the mechanical gaps between tiles created by the segmentation. Such gaps are necessary in order to tolerate launch vibration and thermal expansion.

The requirement to have high detection efficiency for the charged particles and at the same time low efficiency for backsplash-caused signals in the ACD dictates careful optimization of the detection threshold. Therefore it is critical that the detection threshold be highly uniform over the tile area. These requirements point to the need for high light output with good light collection uniformity over the tile area. An additional system requirement is to minimize the inert material in the instrument aperture, making it desirable to locate the light sensors remotely from the tiles.

Thus the basic requirements for each tile detector can be summarized as:

- maximize light yield, providing average detection efficiency of >0.9997 for a MIP,
- provide light production and collection uniform to ± 10% over the tile area,
- implement dual light readout to provide redundancy,
- provide robustness, and
- position the photo-multiplier tubes (PMTs) to minimize inert material in the LAT field of view.

We describe below a design that meets these requirements.

2. Tile detector design

2.1. Design overview

It was decided to use plastic scintillator for the ACD because it is the simplest, most reliable, efficient in charged particle detection and practically inefficient to photons, well-

understood, inexpensive, and robust detector technology; and there was a great deal of experience with the material in space applications. The scintillator tile detectors are made of 1 cm thick polyvinyltoluene (PVT) plastic scintillator ElJen-200, produced by ElJen Technology. The tile thickness choice resulted from a trade-off between minimizing mass (critical for space experiments) and maximizing light yield. The decisive step in the tile design was to choose the readout. The highest light yield could probably have been provided by direct PMT attachment to the scintillator, but the light collection uniformity requirement would have been hard to meet, and the PMTs would have been located in the field of view. It was also unclear how to provide complete ACD coverage of the LAT field of view with such a readout.

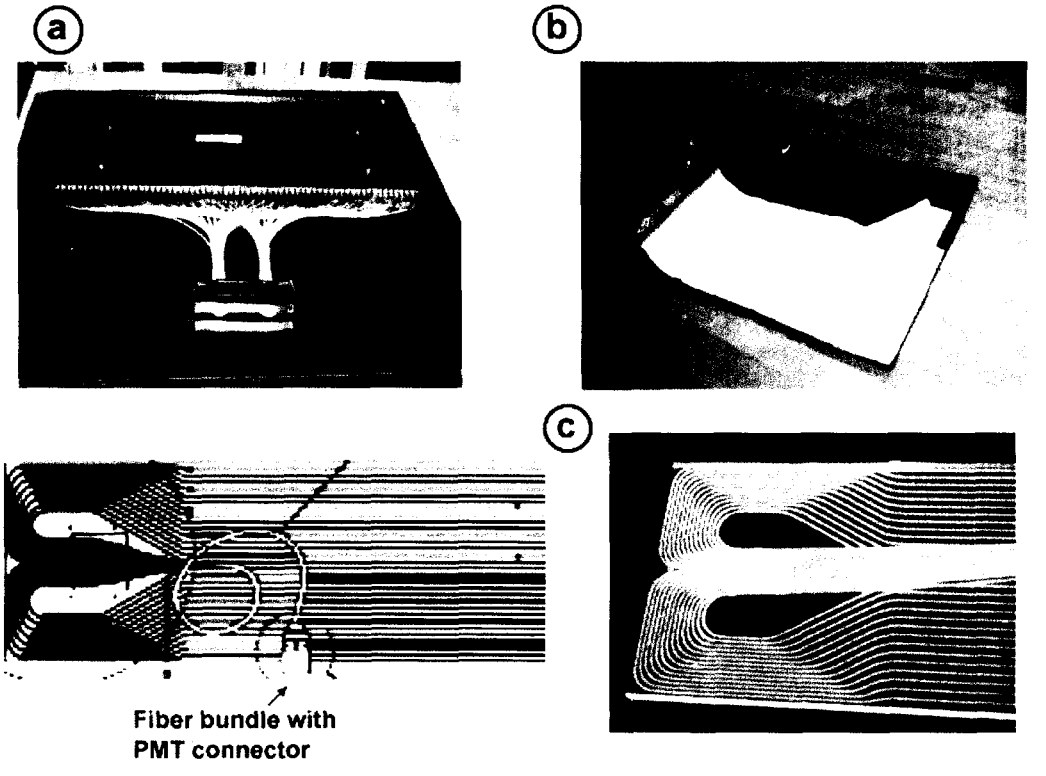

Figure 2. a) "Basic flat" tile, unwrapped. The fiber routing and optical connector are shown; b) "bent" tile with cutout to show the inner light-reflecting wrapping layers and the outer black light-tight layers; c) left half of a symmetrical "long" tile. Left – drawing, right – photo of unwrapped tile

After consideration of different design concepts, including optical light guides, wavelength shifting (WLS) bars, directly coupled PIN photodiodes, etc., it was found that WLS fibers coupled to optical transmission fibers would be the best way to deliver the light to remotely located PMTs. This readout is widely used in accelerator experiments with various modifications depending on the application (e.g. [5-10]). We used the heritage of those studies, but the specifics of a space experiment in general and the LAT

requirements in particular demanded our own investigation and optimization of the detector.

We decided to build three basic shapes for the ACD tiles. In this paper we will discuss these configurations: a rectangular "basic flat" tile 32 cm by various lengths (Fig. 2a), a square 32 cm by 32 cm "bent tile", dimensions to fill that space after bending (Fig. 2b), and a rectangular "long" tile, 170 cm by 17 cm (Fig. 2c).

"Basic flat" tiles are the most numerous in the ACD design. Each tile has 64 keyhole-shaped grooves in which 1 mm diameter WLS fibers are embedded (Fig. 2a). Alternate fibers are gathered and routed to two different PMTs for redundancy. Details of the fiber layout are discussed in 2.3.

A "bent tile" covers the same area as a "basic flat" tile with the added complication that the scintillator has 90-degree bend for use at two edges of the ACD top. These tiles cover the gaps where orthogonal tiles meet (see Fig.1). The bend also enables the fibers from top tiles to turn the corner to reach the PMTs. Special care was required to bend the tiles properly – first not to have the tile edges "bump out" at the bending line due to plastic deformation, and second not to degrade the tile surface during thermal bending. We machined the tile edges after thermal bending to make the edges straight. The bending temperature was optimized at 65°C so as not to degrade the scintillator performance. The light collection uniformity was measured in the bent area and no significant degradation was found.

The "long" tiles, 170 cm long and 17 cm wide, are used around the bottom perimeter of the ACD. Due to the location of these tiles, the fibers must exit the tile surface as shown in Fig. 2c. This requirement creates an additional complexity in the fiber routing. To provide redundant read-out, both sets of WLS fibers have to cover the whole tile. The 26 fibers are placed in curved grooves to collect light from the full tile area and are routed to exit the tile from its large surface. The fiber runs are comparable to the light attenuation length of the WLS fiber. Light attenuation in the tiles will be discussed in section 4.

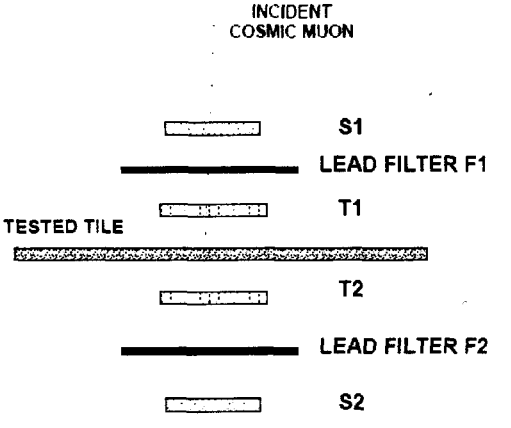

Figure 3. Experimental setup for the efficiency measurement with cosmic muons. The muons are selected by 4-fold coincidence of the signals from S1, S2, T1, and T2 scintillators. Lead filters F1 and F2 are used to remove the electron component.

2.2. Approach to determining tile performance.

For all measurements of scintillation light collection efficiency (light yield) and

uniformity we used cosmic ray muons to measure the detector response. We express the light yield in units of the mean number of photoelectrons emitted from the PMT photocathode by the light produced by a single normally incident MIP in the scintillator. To eliminate dependence on specific PMT parameters (mainly photocathode quantum efficiency), the same physical PMT is used for all comparison measurements.

The approach to measuring the light yield is based on measuring the dependence of MIP detection efficiency upon the signal detection threshold. Fluctuations in the signal amplitude are determined by fluctuations in particle pathlength in the scintillator, ionization losses (Landau fluctuations), and statistical fluctuations in the number of photoelectrons. Measuring the detection efficiency of the MIPs vs. detection threshold, expressed as a fraction of MIP peak position (on a PHA histogram), the light yield, or most probable number of photoelectrons, can be determined by fitting the efficiency dependence by a Poisson distribution with a given mean number. The typical position of the MIP peak on a PHA histogram is at 400-500 ADC bin (after pedestal subtraction) with FWHM of ~300 ADC bins (Landau distribution). The experimental setup removed most pathlength fluctuations. This approach provides an "effective" light yield to characterize the detector efficiency (which is slightly less than the true efficiency).

The experimental setup for this measurement is shown in Fig. 3, where the light yield is measured for the "Tested Tile". Since we want to measure the detection efficiency with high accuracy, a clean sample of quasi-vertically incident muons passing through the central portion of the tile is selected by means of 4-fold coincidence of signals from triggering scintillators S1, S2, T1, and T2 (all 5cm by 5cm). Two 5mm thick lead filters, F1 and F2, are used to remove electrons, and signals from T1 and T2 are required to be more than 20% of the most likely pulse height. This selects muons. An example measurement result is shown in Fig. 4, where the experimental data are fitted by Poisson distributions corresponding to two different mean values.

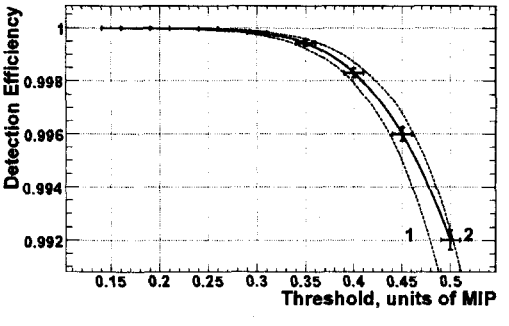

Figure 4. Measured detection efficiency (the solid line through the data points is shown to guide the eye) vs signal detection threshold, expressed in units of MIP fraction. Computed Poisson distributions for mean photoelectron numbers of 20 (dashed line 1) and 22 (dashed line 2) photoelectrons are shown to determine the light yield of the tested tile.

The "long" tile has relaxed requirements for light yield and light collection uniformity; its MIP detection efficiency must be >0.99. Because light attenuation in the long WLS fibers is important for the "long" tile with fiber length comparable to the WLS fibers attenuation length, we measured the MIP detection efficiency and light yield at three points along the tile length – in the center and near the ends.

As mentioned above, each tile must have uniform light collection over

its area. In the design phase we measured the uniformity by using two plastic scintillating hodoscopes specially designed and built for these tests. This technique provided coarse mapping of the tile light yield with 4cm by 4cm pixels. After the ACD integration in the LAT the tile light collection uniformity was accurately measured on a finer spatial scale with the help of the LAT tracker, which reconstructed the position of the particle in the tile with a precision of better than 1mm. With these measurements we determined that the light collection uniformity is within ±5% over the tile area except in a ~2cm border area where the light output gradually degrades to ~80% of its value at the tile center.

2.3. Tile design optimization

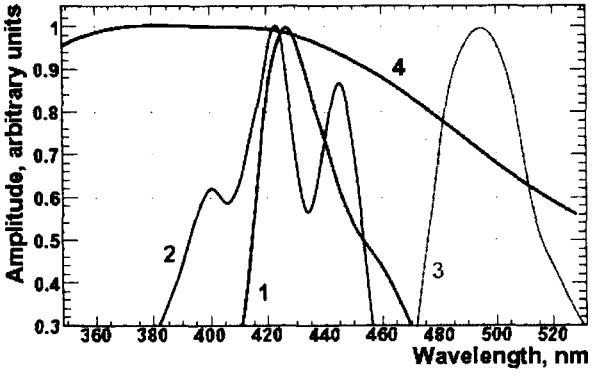

Figure 5. Optical spectra. Line 1 – emission spectrum for ElJen -200 scintillator. Lines 2 and 3 – respectively absorption and emission spectra for WLS fiber BCF-91A, and line 4 – scaled to its maximum value quantum efficiency for Hamamatsu R-4443 PMT

a good match to the BCF-91A maximum absorption wavelength range (410-460 nm) providing maximal light conversion for transmission to the PMT (Fig.5). We also investigated the effect of fiber cladding. It was found that the use of multiclad fibers increased the light yield by 20-25%. For gluing fibers into grooves we used optical epoxy adhesive BC 600 (made by Saint Gobain) as the best match to our scintillator. The CMS experiment [5] also used scintillating tiles with WLS fiber readout, but did not bond the

As mentioned above, WLS fibers, embedded and glued in grooves, collect the light from all three types of tile detectors. This technique, while not the best from the point of view of the amount of light collected, provides the best light collection uniformity over the tile area and allows remote positioning of the PMT.

In order to optimize the light collection in the approach used, the absorption spectrum of the WLS should match the emitting spectrum of the scintillator. The ElJen-200 scintillation light emission peak is at 425 nm and is

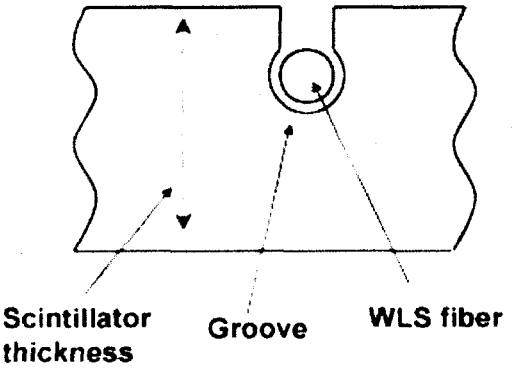

Figure 6. Keyhole-shape groove

fibers; they were simply inserted into keyhole-shaped grooves (Fig.6). We found that bonding the fibers gives at least a factor of 2 increase in light, which was critical for our application but was not so important in CMS tiles where the cost of mass production of thousands of tiles was the driver.

The choice of PMT proved to be very important in optimizing the light output. First, the quantum efficiency even within same type of PMT can vary by a factor of several, so PMT selection helps greatly. The use of "green" WLS fibers is not a good match to the efficiency of a conventional bialkali photocathode (maximum response at ~ 420 nm), because it reduces quantum efficiency at the 490 nm emission peak of BCF-91A (Fig.5). One possibility was to use PMTs with a green-extended photocathode. However, we found that the Hamamatsu R4443 (which was chosen for the project), a ruggedized version of conventional Hamamatsu R647, could not be manufactured in a ruggedized version with green-extended photocathode. We therefore decided to select normal bialkali PMTs for maximum quantum efficiency at 490 nm. It appeared that most of the selected tubes were not the best performers at the nominal 420 nm wavelength but had flatter dependence of quantum efficiency upon wavelength and thus had better quantum efficiency at 490 nm. In the end, the PMTs selected for the project had quantum efficiencies in the range 18-25% at 490 nm.

An optimization study on the depth and spacing of the grooves in the scintillator was performed (Table 1). It was found that embedding the fibers 2mm deep and with 5 mm spacing between grooves gave the best results. Use of two PMTs is dictated by the space experiment reliability requirements to provide redundancy in case of PMT failure. We found that routing alternate fibers to the two different PMTs was optimal,

We studied other design options, such as not embedding the fibers into the scintillator but bonding them directly to the surface of the tile continuously (without gaps between fibers), or to the edge of the tile. The former design, in spite of demonstrating high performance, was rejected due to requiring too many fibers (number of fibers was restricted by the PMT photocathode area). The latter design demonstrated significant decrease in light collection efficiency (about 50%). We also considered other "winding" patterns of grooves in the scintillator that would simplify the fiber bundling and routing outside the tile, but found them to be impractical due to more complicated and expensive groove machining and fiber population.

Fiber Spacing	Light Yield, arbitrary units
2 cm	15.9
1 cm	18.1
0.5 cm	22.0
0.25 cm	20.2
continuous	23.3

Table 1. Comparison of light yield for different fiber layout

Embedding the fibers in keyhole-shaped grooves [5] provides convenience and confidence in securely holding the fibers in the grooves. It proved to be especially important in bent tiles, where the fibers could easily escape from the grooves in the

bending zone if they were not secured by the key shape of the grooves. In order to protect the fibers against cracking at the exit point from the tiles, thin flexible tubing about 2 cm long was placed over each fiber.

If the fibers are read out from one end (as for "basic flat" and "bent" tiles), the treatment of the unused end is important to return some portion of the light to the collection end. We found that aluminizing the end yielded ~20% higher light collection in comparison with only polished fiber ends, so all open fiber ends were aluminized.

2.4. Tile detector packaging

In accordance with the requirement of minimal inert material in the sensitive area, each tile is not boxed or framed but rather is enclosed within a light-tight wrapping. This constraint created substantial problems in finding the proper materials and establishing the wrapping procedure. The inner wrapping layer must provide good light reflection, and the outer layer must provide light tightness (see Fig. 2b). It is important to have the surfaces of the scintillator polished so that they reflect at least 50% of the scintillation light inside the scintillator. The inner wrapping, in its turn, has to maximize the return of escaping light to the scintillator. We studied three different wrapping materials: Tyvek, Tetratex, and Polyester (our choice was limited by the materials permitted for the use in space experiments). We found that the best results can be achieved with two layers of 0.25mm thick Tetratex (a teflon-based material).

Light from external sources (sunlight, in particular) must be prevented from entering the tiles. The external wrapping, providing light tightness, is two layers of 50 μm thick black Tedlar. Light tightness measurements that we made demonstrated that the two layer wrapping absorbs practically all incident light, with the remaining light leak corresponding to the signal from less than 0.5 photoelectron, limited by the measurement technique sensitivity.

Because the tile detectors must operate in vacuum, proper venting of the tile envelope must be provided. This requirement created additional difficulty due to conflicts with the light tightness requirement. In order to provide the venting, the process of wrapping with overlapping layers was carefully designed. A fraction of the seams in the outermost wrapping layer were left partially untaped to allow venting to take place.

Since the tile design is "frameless", the tile mounting was an issue. It had to take into account the required minimization of dead areas, or gaps, between adjacent tiles. The final design has every tile mounted to the ACD structure by four 3mm diameter screws that go through the scintillator. The "long" tiles have 14 screws. The holes are drilled between the fibers with special care not to have the response distorted in the vicinity. We investigated whether the scintillator can be damaged by the screws during mechanical vibration and found no performance degradation after those tests. The effect

of the dead area caused by the holes was studied and determined to cause degradation in detection efficiency for an isotropic incident flux of less than 0.00005. Light sealing in the vicinity of the screws was provided by the use of special black rubber washers.

2.5. Light transport from the tiles to the PMTs

The design of ACD requires that the PMTs are positioned at different distances, up to about 1.5 m, from the tiles. We considered two approaches to delivering the light from the tile to PMT. The first option was to run WLS fibers all the way, and the second was to mate the WLS fibers to clear optical fibers or "cables". We measured the attenuation length of WLS fibers to be ~1.6 m, slightly changing along the fiber according to the distance from the tile. The attenuation length for clear fibers was measured to be ~6 m. Both of these numbers were obtained for our relatively short fiber runs and can be larger for longer fiber lengths. To maximize the amount of scintillating light delivered from the scintillator to the PMT, the optimal design uses the first option for the tiles with total fiber runs less than 40 cm, and the second option for longer fiber runs. For the clear fiber cables, 1.2 mm diameter BC-98 fibers (from Saint-Gobain, formerly Bicron) fibers are used. The larger diameter (WLS fibers are 1 mm diameter) allows for the tolerance in fiber mating alignment.

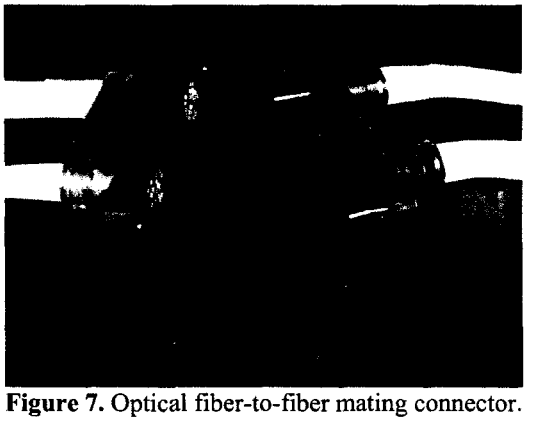

Figure 7. Optical fiber-to-fiber mating connector. Alignment pins are seen on the right (clear fiber) side. Opaque tubing that surrounds the fiber bundles has been removed for clarity.

We investigated two options for fiber mating: 1) optical mating in specially designed connectors, and 2) thermal coupling as used in CMS [5,11]. No grease was allowed due to the space flight requirements. For our detector we chose the former method to permit for easy de-mate and re-mate if needed to simplify ACD integration and servicing. No significant difference was found in the light conduction efficiency between these two options, both of which suffer 15-20% light loss at the point of fiber mating.

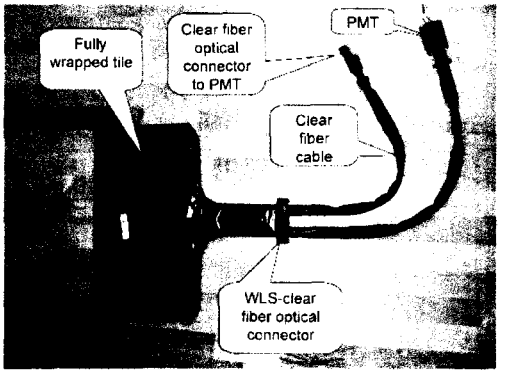

Figure 8. Assembled "basic flat" tile.

One issue that arose was how to bundle the fibers at the output from

the tile and provide light tightness at the point where the fiber bundle split in two for the two redundant PMTs. A special interface was designed with two versions. An optical connector (Fig. 7, also seen in Fig. 2) does fiber mating and consequently requires precise machining to provide fiber alignment and fiber end polishing to provide the best light conduction. A pass-through connector (for those tiles where the light is delivered by only WLS fibers) is needed only to provide light tightness in the transition point from the tile to the fiber bundles. Its design is similar to that of the mating connector, but it consists of only one pass-through part. Both of those connector types split the fibers from a tile into two bundles, to be routed to different PMTs, and provide venting as well. Fiber bundles and clear fiber cables are inserted in Sumitube black tubing (made by Sumitomo Electric). The tubing provides light tightness and connects to the PMT housing. Fig. 8 shows the whole tile-to-PMT assembly.

3. Tile fabrication

Fabrication of the tiles is a critical step in achieving high performance of the tiles and implementing all design findings. The intended 10 year lifetime in space requires that a clean environment be maintained during tile fabrication, to prevent scintillator crazing from foreign residuals (e.g. human and mechanical oil). Prototyping and fabrication of the tiles was performed at Fermi National Laboratory. In this section we describe the main steps in tile fabrication.

Plastic scintillator sheet inspection and preparation: Initial inspection of the scintillator was performed in order to find any obvious damage or flaws, before any operations were performed. Special care was taken to check the scintillator sheet flatness and thickness uniformity, both to be within 0.15mm. Final scintillator quality inspection was performed when the scintillator was unwrapped for cutting to size. Rubber gloves were mandatory during handling of unprotected scintillator. No scratches or scintillator damage were allowed. After cutting the tiles to size the edges were diamond polished, and the mounting holes were drilled. At this point each tile was assigned an ID number and traveler, used as an aide in the assembly steps. Each step was signed off by the technician that performed the step, as well as a Quality Assurance representative.

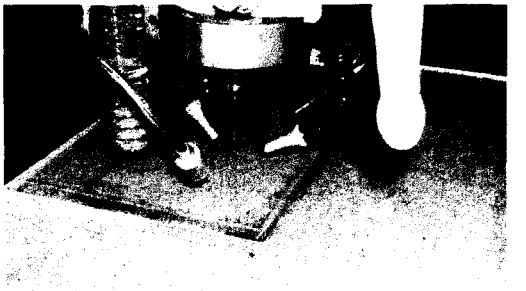

Figure 9. Tile groove cutting.

Groove cutting. This operation is critical for the maximization of light collection. Proper tools and optimized cutting speed are the decisive factors. An improper tool or cutting speed too high can cause optical defects, in particular scintillator "melting" which

is essentially impossible to remove. Grooves are cut by Axxiom CNC according to the files programmed for each tile configuration. Special care was taken to cool the cutting area to prevent scintillator melting (Fig.9). The Axxiom tool speeds were adjusted daily depending on temperature and humidity. Test cuts were preformed to assure the cuts were clean and the tool speeds were adjusted for optimizing the quality of the cuts. Several passes were preformed for each groove to improve the quality of the cuts to allow the best transition of the scintillating light through the walls of the cuts.
After completion of groove cutting the tiles are annealed at 70C for 3 hours. This removes remaining stress in the scintillator which can cause crazing and consequent performance degradation.

Tile bending. This operation was performed to create the "bent" tiles. The tile forming fixture was cleaned and preheated before each use. The tile bending edge is preheated to 65C and maintained throughout the forming process. The tile was placed in a preheating fixture and heated for approximately 10 minutes. Tile was removed from the preheating fixture and placed on the forming fixture. A forming sheet was placed over the tile forcing it to contour with the fixture. Weights were added and the fixture/tile was allowed to return to the ambient room temperature. Once cooled tile was inspected for any crazing or damage from the process.

Fiber preparation and gluing. WLS fibers are the key element in the tile detector, and tile light yield critically depends on their performance. Fibers with damaged outer cladding, which can be found visually by characteristic bright rings, were removed during the initial fiber inspection. The next step was to mirror the fiber ends. The fiber ends were first ice polished (polished in frozen state), then sputtered with aluminum and finally the mirrored end was coated with protecting chemical and cured for 15 min with UV lamps. This process secures the best internal reflection and long time stability. .

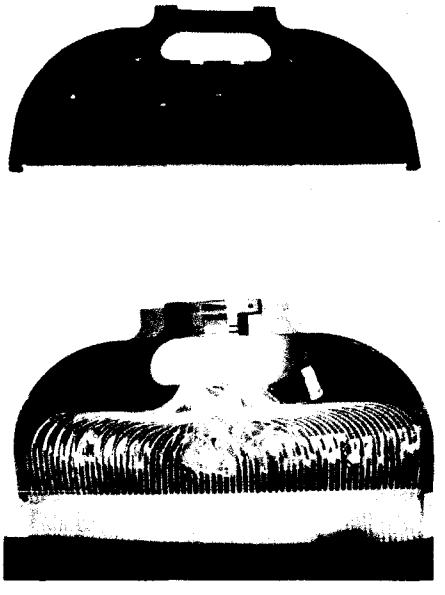

Figure 10. Fiber routing. Upper panel – routing template. Lower panel – fibers routed on the template.

The next operation was gluing the fibers into the grooves. Special care must be given to eliminating air bubbles in the glue, which dramatically reduce the collected light. Prior to gluing the fibers into the grooves, the entire tile surface was temporary covered by 3M8901 tape to prevent the glue from spilling out of the grooves and degrading the internal reflection performance of the tile surface. The BC-600 optical epoxy was mixed and

then set into a vacuum chamber for several minutes to remove all air from the mixture. The mixture was then transferred to an injection applicator and injected into the fiber grooves. Slowly injecting the mixture was important to allow for time for the air in the groove to release and be pushed out. A slight movement of the fiber may be needed to help loosen the trapped air inside the groove to allow it to be pushed out.

Optical connector installation. Fibers were routed to the connector alternating every other fiber to one of the two connector outlets (Figs. 2a, 7 and 10). The demanding requirement in fiber routing was that the dimension "d" on Fig.10, lower panel, was critical and must be kept under up to 23mm for some of the tiles due to the ACD mechanical constraints. Taking into account that the allowed minimum fiber bending radius is 20-25 mm, this represented a challenge. In order to accomplish it, a special routing template was made, different for each tile type (Fig.10, upper panel). Use of these templates assured that the fiber length from the tile to the connector was set right, the fibers were all relaxed and that no fiber was tighter than the others. Once the fibers were in place, they were taped to the template to prevent movement. The next step was inserting the fibers in the connector holes (also ordered to minimize fiber crossing) and filling the holes with BC 600 glue using a syringe.

After the BC 600 glue was cured, the routing template with the tile and connector was kept in an oven for 3 hours at 70C for annealing, followed by return to room temperature over 12 hours interval. Fibers stresses were relieved during this operation. Finally, polishing was performed on the fiber/connector ends. Once the fibers were frozen the ends were polished with an Ultra High Speed Diamond cutter. After polishing each batch was inspected under magnification for any damage or smudges. This assures that the surfaces met specifications and can be used. The tile after this step is shown in Fig.2a.

Tile wrapping. The final operation in tile production was wrapping. As described in Section 2.4, the wrapping includes two inner light reflecting layers of white Tetratex, and two outer light tight layers of black Tedlar. After wrapping, the tile was subjected to a light tightness test. This test was performed by connecting a PMT to the optical connectors, and comparing the signal rate (with the discriminator threshold set to ~0.5 photoelectron) with the tile covered by light tight blanket and without it. The tile was considered to be light tight if the difference was less than the statistical error in the rate measurement.

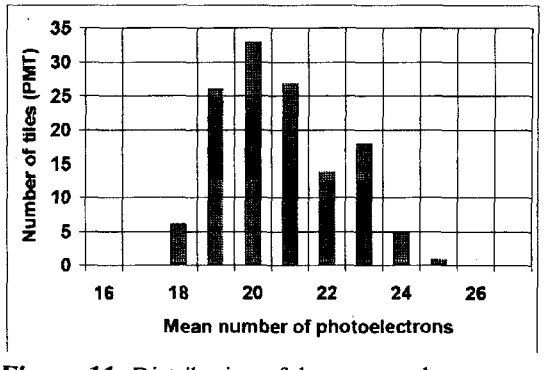

Figure 11. Distribution of the measured photoelectron yield for 170 ACD tile channels ."Long" tiles excluded; two signals (PMT) from each tile.

4. Discussion of the tile detector performance

As a result of numerous optimization studies, the light yield performance of 85 tile detectors of

different size and shape (excluding the long tiles), is shown in Fig.11 (each tile shown twice because of two PMTs), with a mean value of ~ 20 photoelectrons. These results were obtained from a setup with fiber mating optical connector and with ~ 20cm long clear fiber cable extension. We estimate that in this setup the connector and clear fiber cable acting together reduce the light by ~ 30% with respect to that coming out of the tile. Essentially no difference in performance was found between the "basic flat" and "bent" tiles. It is important to note that Fig. 11 shows the light yield after splitting the light between two PMTs, so it would approximately double if the tile fibers were viewed by a single PMT. A tile with two PMTs operating in "OR" demonstrates muon detection efficiency of >0.9999 with the detection threshold set to 0.3 MIP, and >0.999 in the case of one PMTs failure (results were obtained with cosmic muons as described in Section 2.2). Taking into account attenuation in the fiber cable and the light splitting to two PMTs, we estimate that the light yield for our tile detectors would be ~ 60 photoelectrons if they were read out by a single PMT without the optical fiber coupling. All of these measurements were made with the same relatively poor testing (non-flight) PMT with quantum efficiency of ~15% at 490 nm. The flight ACD utilizes PMTs selected for quantum efficiency >19%, which raises our estimate of single tile light yield to ~ 75 photoelectrons.

The tile detectors design was also tested in accelerator beams ([4, 12, 13]) and in a balloon flight [14], confirming the performance measurements and demonstrating high reliability and easy handling. It is not easy to compare our results directly with those reported by other groups because the performance is strongly affected by the application-driven detector designs. Various authors report light yields for MIPs achieved by different plastic scintillator detectors with WLS fiber readout, ranging from a few to about 100 photoelectrons per centimeter of scintillator thickness [5-10]. Our detectors are therefore among the best.

Fig. 12 shows the light output profile (PHA histogram) for the tile, obtained with a relativistic carbon beam [13]. The data were taken using the "high" range of ACD electronics, which allows us to register high amplitude signals from heavy cosmic ray nuclei. The signal for carbon is ~700-800 photoelectrons so the tile energy resolution is determined practically only by the ionization losses fluctuation and reaches the value of ~15% FWHM. This energy resolution makes possible to see the effect of the WLS fibers ("dead" material) embedded in the tile: the fiber pitch is 5 mm.

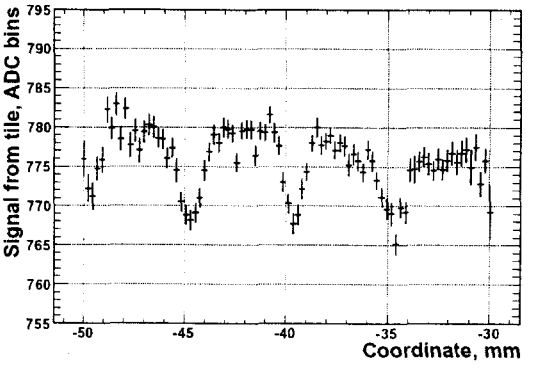

Figure 12. Signal profile for the central part of a tile (across the fibers) obtained with a carbon beam. The dips separated by ~ 5mm correspond to the fiber pitch, and resulting from thinning of the tile by the fiber groove depth.

Light yield for a "long" tile is

shown in Fig. 13 (upper panel) for a PMT viewing the tile from one end as a function of the muon impact coordinate. The PMT on the opposite end has similar performance. Fig. 13 (lower panel) shows the resulting normal incidence MIP detection efficiency vs. the muon traversal coordinate along the tile with detection threshold set to 0.3 of a MIP mean value. The flat line representing the sum signal does not fell below 0.9998, demonstrating high and uniform detection efficiency for such a long scintillator paddle. It is also seen that for only one PMT the MIP detection efficiency is >0.98 over the entire detector area.

In order to assure that the assembled flight tile detectors meet the requirements for use in a space flight experiment, a number of environmental and mechanical tests were performed. Our detectors successfully passed all of them. We briefly mention here the tests which are essential. Vibration tests included random vibrations along three axes, from 20 Hz to 2000 Hz , and sine burst normal to the tile plane. After each axis vibration the total light yield and light yield mapping (with 4cm by 4cm pixels, see Section 2.2 for details) were measured. Light yield mapping was needed to reveal possible damages in fiber gluing which would affect the light yield from particular tile area. No detectable degradation was observed. A thermal cycling test was performed to assure that there will be no defects/cracks in the fiber themselves or their gluing due to the thermal stress. No significant light yield change was found after 440 cycles over the temperature range from -60C to +45C. A vacuum test was performed in order to determine possible damage to the light tight envelope during the rapid pumpdown from normal atmospheric pressure to vacuum. No light leaks were observed after 10 cycles.

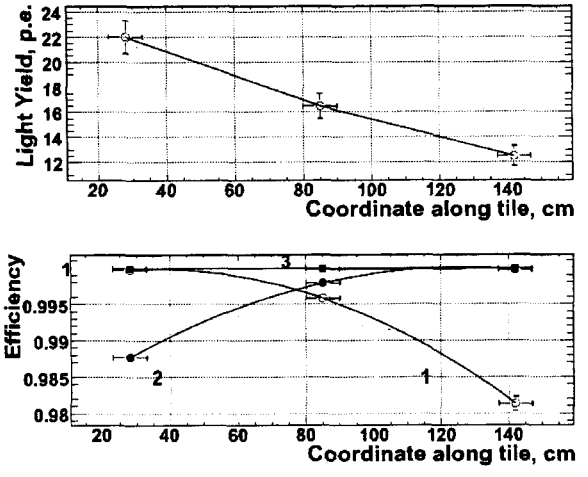

Figure 13. Performance of the "long" tile.
The upper panel shows the light yield obtained at one end of the tile, vs. the distance along the tile to the muon traversal point.
The bottom panel shows the efficiency of muon detection vs. the muon traversal point for the PMT at the "0 cm" end (line 1, open circles), at the opposite end (line 2, filled circles), and for both PMT operating together (line 3, filled squares).

5. Conclusions and acknowledgements

We designed, fabricated, and investigated the performance of scintillator tile detectors with WLS fiber readout of various sizes (from 450 cm^2 to 2500 cm^2) and shapes (flat and bent). Intended for use in the space gamma-ray observatory GLAST, the detectors meet all the requirements for a space experiment and are optimized to have maximum light yield combined with highly uniform spatial response. The tiles are read out using variable lengths of flexible light transmitting cable, made of clear fibers that are mated to the tile WLS fibers by custom designed optical connectors. This allows the use of remotely positioned PMTs outside the active

area of the detector. Such a design would be useful in an experimental setup where the PMT cannot be placed next to the detector due to integration constraints or magnetic field issues. Each tile is read out by two redundant PMTs that operate simultaneously in an "OR" mode, achieving >0.9999 MIP detection efficiency. Were redundant readout not required, the scheme presented here could be easily modified for a single PMT, doubling the number of collected photoelectrons in a single PMT. We achieved an average effective light yield of ~ 20 photoelectron per 1cm of plastic scintillator for MIP and dual readout with optical connectors and ~ 20 cm long fiber cables. In the case of single PMT readout with optimized optical transmission and carefully selected PMTs the light yield could reach at least 75 photoelectrons. The light collection is uniform over each tile area and is well within ±5% of its mean value, with some decrease at the tile edges.

The authors express their gratitude to Eileen Hahn, John Korienek, John Blomquist and others from the Detector Laboratory at FNAL for their excellent work on the tile detector fabrication. We thank ACD technicians at NASA Goddard Space Flight Center (Deneen Ferro, Bill Daniels, Nick Kwiatkovski, Tom Huber) and the entire LAT ACD team for their critical contributions in all steps of tile detector design, fabrication and testing. We are grateful to the Hamamatsu group, and especially Andrew Allen and Yuji Yoshizawa for providing excellent phototubes that were specifically tailored to meet our goals. Support and suggestions from LAT team members and the members of LAT Calibration and Analysis group in particular, are greatly appreciated. We especially thank our LAT internal reviewers Gary Godfrey and Niccola Mazziotta for careful reading of the manuscript and providing valuable comments and suggestions.

6. References

1. W. B. Atwood et al., in preparation
2. E. B. Highes et al., IEEE Trans. Nucl. Sci. NS-27 (1980), 364
   C. E. Fichtel et al., Astron. Astrophys. Suppl. 120 (1996), 23
3. A. A. Moiseev et al., Astroparticle Physics, 27 (2007), 339
4. A. A. Moiseev et al., Astroparticle Physics, 22 (2004), 275
5. S. Aota et al., NIM A352 (1995), 557
6. A. P. Ivashkin et al., NIM A394 (1997), 321
7. O. Mineev et al., NIM A 494 (2002), 262
8. M. Beddo et al., NIM A 499 (2003), 725
9. M. D. Diwan et al., Nucl. Phys. B (Proc. Suppl.), 123 (2003), 272
10. S. Kuhlmann et al., NIM A 518 (2004), 39
11. K. Hora et al., NIM A 348 (1994), 139
12. W. B. Atwood et al., NIM A 446 (2000), 444
    E. do Couto e Silva et al., NIM A 474 (2001), 19
13. L. Baldini et al., First GLAST Symposium, Editors Ritz, Michelson and Meegan, AIP 921 (2007), 190
14. D. J. Thompson et al., IEEE Trans. Nucl. Sci. 49 (4) (2002), 1898